ADVANCED FUNCTIONAL MATERIALS
www.afm-journal.de

Gelation of Uniform Interfacial Diffusant in Embedded 3D Printing

Sungchul Shin, Lucia G. Brunel, Betty Cai, David Kilian, Julien G. Roth, Alexis J. Seymour, and Sarah C. Heilshorn**

While the human body has many different examples of perfusable structures with complex geometries, biofabrication methods to replicate this complexity are still lacking. Specifically, the fabrication of self-supporting, branched networks with multiple channel diameters is particularly challenging. Herein, the Gelation of Uniform Interfacial Diffusant in Embedded 3D Printing (GUIDE-3DP) approach for constructing perfusable networks of interconnected channels with precise control over branching geometries and vessel sizes is presented. To achieve user-specified channel dimensions, this technique leverages the predictable diffusion of cross-linking reaction-initiators released from sacrificial inks printed within a hydrogel precursor. The versatility of GUIDE-3DP to be adapted for use with diverse physicochemical cross-linking mechanisms is demonstrated by designing seven printable material systems. Importantly, GUIDE-3DP allows for the independent tunability of both the inner and outer diameters of the printed channels and the ability to fabricate seamless junctions at branch points. This 3D bioprinting platform is uniquely suited for fabricating lumenized structures with complex shapes characteristic of multiple hollow vessels throughout the body. As an exemplary application, the fabrication of vasculature-like networks lined with endothelial cells is demonstrated. GUIDE-3DP represents an important advance toward the fabrication of self-supporting, physiologically relevant networks with intricate and perfusable geometries.

1. Introduction

Channels with intricate geometries are critical for the function of many tissues throughout the human body, including vascular networks, lymphatic vessels, airway channels, and the gastrointestinal tract.[1–5] These naturally evolved, perfusable geometries have inspired bioengineers to fabricate mimetic structures for use in organ-on-a-chip models,[6–8] as tissue engineered therapies,[9,10] and for studying the role of physical forces in regulating healthy and diseased cellular function.[11,12]

Compared to micromolding or microfluidics, 3D printing of biomaterial inks has emerged as a technique to create perfusable networks with user-specified channel paths that can be easily reconfigured.[13,14] In one bioprinting strategy for channel formation, a tube-like structure is created through direct layer-by-layer printing of the channel walls.[15–17] While this allows for fabrication of branched networks, the structures are prone to leakage due to insufficient adhesion between layers, and the resulting surfaces and interfaces are typically not smooth. To address these limitations, coaxial extrusion can be used to fabricate perfusable channels by directly printing hollow filaments from concentric nozzles.[18–20] However, since the inner and outer diameters are set by the nozzle geometry, the final printed structure cannot include interconnected branch points. This technique is therefore limited to single-lumen geometries of fixed diameter. As an alternative approach, extrusion printing of a sacrificial ink enables patterning of void spaces within a bulk material to form interconnected lumens with smooth inner surfaces.[21–23] In contrast to core–shell extrusion, this sacrificial ink strategy results in perfusable structures without a vessel-like shell. As such, this method cannot be used to

S. Shin, B. Cai, D. Kilian, S. C. Heilshorn
Department of Materials Science and Engineering
Stanford University
466 Lomita Mall, Stanford, CA 94305, USA
E-mail: sungssc@snu.ac.kr; heilshorn@stanford.edu

S. Shin
Department of Agriculture
Forestry, and Bioresources
Seoul National University
Seoul 08826, Republic of Korea

L. G. Brunel
Department of Chemical Engineering
Stanford University
466 Lomita Mall, Stanford, CA 94305, USA

J. G. Roth
Institute for Stem Cell Biology and Regenerative Medicine
Stanford University
466 Lomita Mall, Stanford, CA 94305, USA

A. J. Seymour
Department of Bioengineering
Stanford University
466 Lomita Mall, Stanford, CA 94305, USA

The ORCID identification number(s) for the author(s) of this article can be found under https://doi.org/10.1002/adfm.202307435

DOI: 10.1002/adfm.202307435

form self-supporting networks. To fabricate self-supporting tubular structures, a new paradigm is emerging that relies on control of the liquid–liquid interface between the printed ink and a support bath. In one example, complex coacervation between oppositely charged polyelectrolytes resulted in spontaneous formation of vessel-like shells;[24] however, this technique is limited to materials that have complementary charge. In a second example, diffusion of gelation initiators from a prefabricated, sacrificial gelatin core was used to form multilayered channel walls,[25] although this technique required manual manipulation (i.e., successive immersion into gel precursor solutions) and hence was best suited for larger-diameter structures.

Leveraging this principle of interfacial gelation, we developed a versatile method for the 3D printing of perfusable, self-supporting channels with interconnected branch points and predictable, user-specified diameters that is compatible with a range of different biomaterials; we term this method Gelation of Uniform Interfacial Diffusant in Embedded 3D Printing (GUIDE-3DP). We demonstrate the versatility of this platform to be adapted for multiple materials and physiochemical hydrogel cross-linking mechanisms, the independent tunability of both the inner tube diameter and outer shell diameter of printed channels, and the ability to fabricate seamless junctions at branch points. Finally, to exemplify the use of GUIDE-3DP for creating physiologically relevant structures, networks of perfusable channels are fabricated with an endothelial cell lining to mimic vasculature.

2. Results and Discussion

Embedded 3D printing is an additive manufacturing strategy in which inks are extruded within a support material, decreasing deformation due to gravity or surface tension and thus enabling the printing of inks into complex geometries.[26,27] In our GUIDE-3DP technique, we leverage the predictable diffusion of cross-linking reaction-initiators, released from sacrificial inks within the support material, to rapidly create perfusable, self-supporting networks with precise control over the branching geometry and vessel dimensions (**Figure 1**). In this strategy, a cross-linkable gel precursor is employed both as the support matrix for microextrusion printing as well as the material that eventually comprises the vessel walls. A sacrificial ink containing a cytocompatible reaction-initiator is printed into the gel precursor. Following printing, the reaction-initiators diffuse radially and uniformly across the ink interface and into the surrounding gel precursor (Figure 1a, left panel). The cross-linking reaction occurs only in regions where the gel precursor is in contact with the reaction-initiator, which can be selected to either induce spontaneous cross-linking or to require an external trigger such as light activation (Figure 1a, middle panel). Finally, the sacrificial ink and un-cross-linked support material are removed, resulting in a self-supporting, perfusable printed structure (Figure 1a, right panel).

As a first demonstration, light-cross-linkable gelatin methacryloyl (GelMA) was selected as the gel precursor support material with a slurry of gelatin microparticles loaded with a photoinitiator (lithium phenyl-2,4,6-trimethylbenzoylphosphinate, LAP) as the sacrificial ink. When a filament of the sacrificial ink is printed within the GelMA support material (Figure 1b), the encapsulated reaction-initiator (i.e., LAP) begins to diffuse radially away from the ink. Upon LAP activation with ultraviolet (UV) light, a continuous shell of cross-linked GelMA is formed around the sacrificial ink, which can then be removed after melting, resulting in a perfusable channel (Figure 1c, panels i and ii). In contrast to the GUIDE-3DP approach, previous layer-by-layer demonstrations of printing self-supporting channels[15–23] typically result in surfaces that are discontinuous and prone to defects that may cause leakage due to gaps or delamination of the additive layers (Figure 1c, panels iii and iv) and do not allow the shell diameter to be adjusted independently of the size of the printing needle and the resulting mass flow. Moreover, these traditional additive manufacturing strategies are time-intensive, since multiple passes are required to print a single channel, and limited in their ability to tune the channel dimensions, since the wall thickness cannot be less than the thickness of a single printed filament. GUIDE-3DP overcomes all three of these constraints. The channel surface is uniform since the diffusion of the reaction-initiator into the support material is uniform; the total print time is reduced since the nozzle moves along the print path only once for a single channel; and the shell thickness is controlled by setting the diffusion time. Moreover, the GUIDE-3DP strategy is amenable to a broad range of polymers and cross-linking mechanisms. Previous strategies to fabricate self-supporting, vascular-like networks have included an aqueous-in-aqueous embedded bioprinting method using interfacial coacervation.[24] As this strategy imposes stringent requirements on the properties of bioinks and support materials (i.e., polycations and polyanions that form complex coacervates), they are not generalizable to a broad library of materials as is possible with GUIDE-3DP. On the other hand, recent developments in digital light processing and volumetric bioprinting have enabled the fabrication of perfusable branched channels with high resolution and tailorable architecture.[28] However, the availability and tunability of cytocompatible resins and suitable printers for these approaches remain limited,[29] while GUIDE-3DP can be conducted with any common microextrusion printer and is applicable to a wide range of materials that are readily available and well characterized. To demonstrate the versatility of our strategy, we formulated seven different gel precursor materials to enable cross-linking by the following mechanisms: 1) photo-cross-linking with UV light for GelMA, hyaluronic acid methacrylate (MeHA), and poly(ethylene glycol) diacrylate (PEGDA), 2) cross-linking with small molecules for alginate and polyacrylamide (PAAm), and 3) enzymatic cross-linking for fibrin and gelatin. All seven distinct support material/sacrificial ink combinations were successfully used for GUIDE-3DP fabrication of perfusable structures (Figure 1d). A table detailing the material composition and printing parameters for all constructs in this paper is presented in Table S1 (Supporting Information).

The GUIDE-3DP strategy is enabled by the material properties of the sacrificial ink and gel precursor support material. As the hydrogel component of the sacrificial inks for GUIDE-3DP, we chose a slurry of gelatin microparticles (**Figure 2**). The gelatin microparticles (mean diameter of 18.0 ± 4.0 μm) were fabricated with complex coacervation and concentrated by filtration to form a jammed microparticle ink (Figure 2a,b). After comparing the rheological analysis of concentrations ranging from 4 to 10 wt%, the 8% gelatin microgel ink was identified as having the viscoelastic properties required for printing smooth filaments

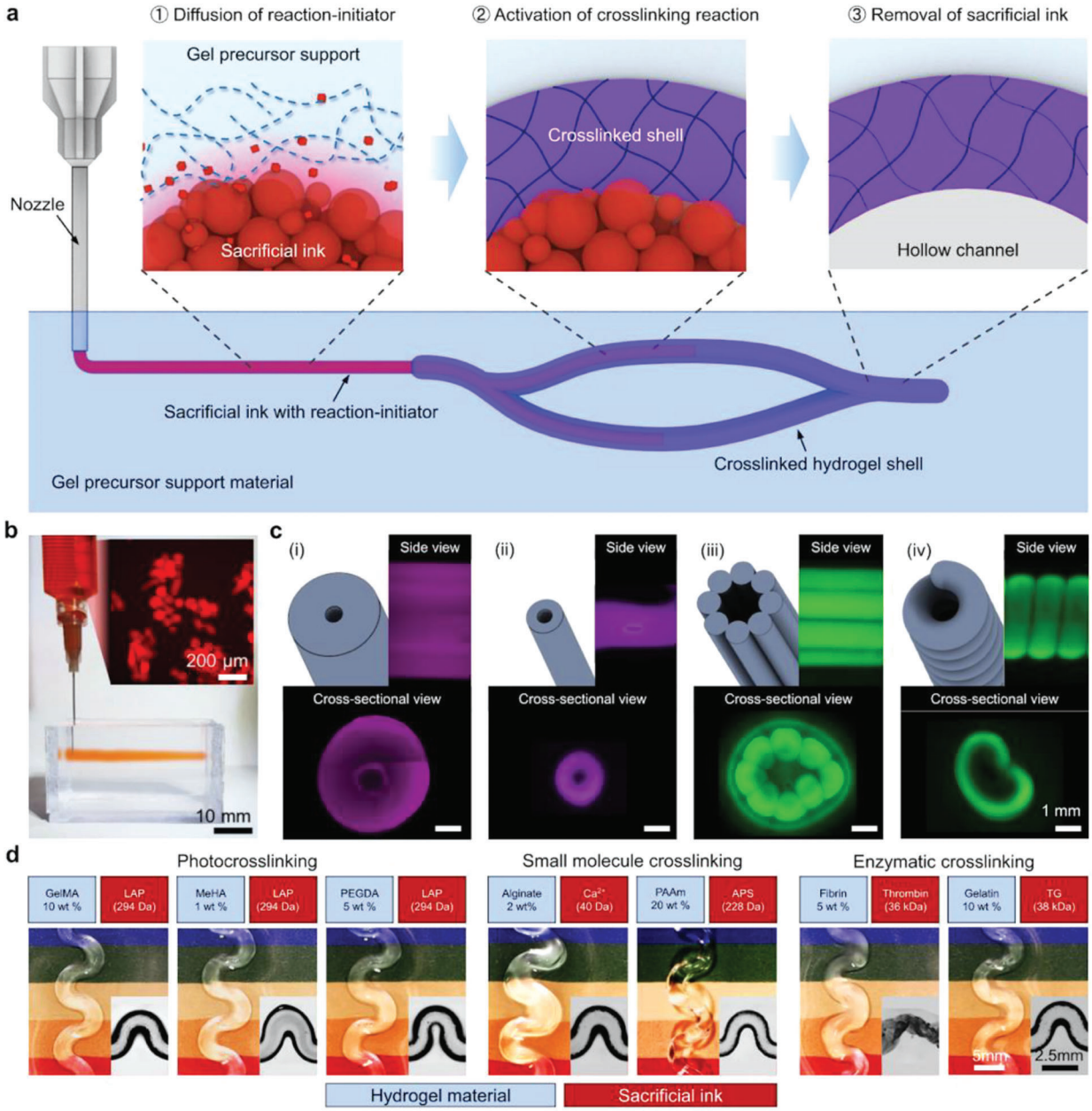

Figure 1. The Gelation of Uniform Interfacial Diffusant in Embedded 3D Printing (GUIDE-3DP) method. a) Sequence of key steps in the GUIDE-3DP method. 1) A sacrificial ink containing a reaction-initiator is extruded into a corresponding gel precursor support material, and the reaction-initiator diffuses out of the sacrificial ink and into the gel precursor. 2) The cross-linking reaction occurs in areas that contain both the gel precursor and the reaction-initiator, forming a shell of cross-linked gel. 3) The sacrificial ink and unreacted gel precursor material are removed, resulting in a printed structure with an open, hollow lumen. b) A sacrificial ink composed of gelatin microparticles (inset) is extruded into a GelMA support material. c) The GUIDE-3DP method (panels i, ii) allows for the fabrication of seamless hollow channels, unlike the conventional approach of direct, layer-by-layer printing of tubular constructs (panels iii, iv). d) The GUIDE-3DP method is amenable to a variety of common biomaterials and cross-linking approaches, demonstrated here with photo-cross-linking (GelMA/LAP, MeHA/LAP, PEGDA/LAP), small molecule cross-linking (alginate/calcium ions (Ca^{2+}), PAAm/ammonium persulfate (APS)), and enzymatic cross-linking (fibrin/thrombin, gelatin/transglutaminase (TG)).

within the GelMA support material (Figure S1a,b, Supporting Information). Specifically, the 8 wt% gelatin microparticle slurry demonstrated important sacrificial ink characteristics, including 1) yield stress and shear-thinning behavior (Figure 2c,d), which enables extrusion through the print nozzle; 2) rapid self-healing (Figure 2e), which limits ink spreading and improves print resolution; and 3) controllable sol–gel phase transition, melting at temperatures above 34 °C (Figure 2f), which facilitates its removal from the final print. This 8 wt% microgel ink has a zero shear viscosity of ≈800 Pa s and a flow index n of 0.8 obtained

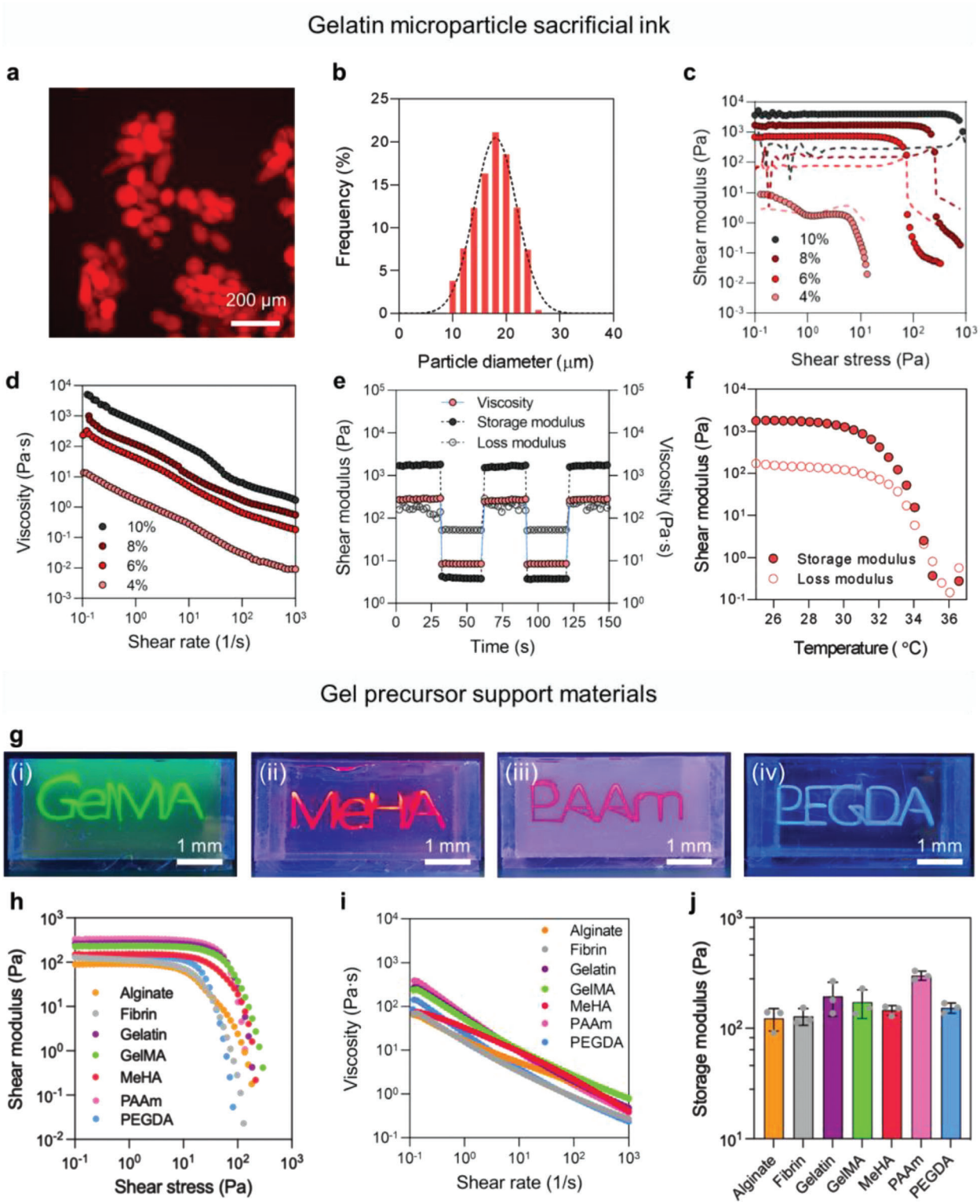

Figure 2. Material properties of the sacrificial ink and gel precursor support materials that enable GUIDE-3DP. a) Fluorescence images of the gelatin microparticles used in the sacrificial ink prior to jamming, stained with rhodamine. b) Distribution of gelatin microparticle diameters. Formulations of the gelatin microparticle sacrificial inks ranging from 4 to 10 wt% exhibit c) yield stress (storage modulus G' represented with filled circles; loss modulus G'' represented with dashed lines) and d) shear-thinning behavior. The gelatin microparticle sacrificial ink (8 wt%) exhibits e) self-healing and f) thermoreversible behavior. g) Sample prints of selected gel precursor support materials i) GelMA, ii) MeHA, iii) PAAm, and iv) PEGDA. Each gel precursor support material (alginate, PAAm, GelMA, MeHA, PEGDA, fibrin, and gelatin) with 2 wt% of the viscosity modifier Aristoflex AVC added has h) a yield stress, i) shear-thinning behavior, and j) storage moduli between 100 and 1000 Pa in the linear viscoelastic regime.

by fitting to the Herschel–Bulkley model (Table S2, Supporting Information), which provides a measure of its shear-thinning behavior. Similar to other granular inks, the 8 wt% gelatin microgel ink had excellent print fidelity compared to a nongranular gelatin ink (Figure S1c,d, Supporting Information), presumably due to the low rheological loss factor that is common for granular fluids.[30]

We next demonstrated that by changing the reaction-initiator within the sacrificial ink, we can construct prints with a variety of gel precursors and cross-linking mechanisms using GUIDE-3DP (Figure 2g). We achieved suitable rheological properties of each gel precursor support material (alginate, PAAm, GelMA, MeHA, PEGDA, fibrin, and gelatin) by adding Aristoflex Ammonium Acryloyldimethyltaurate/VC Copolymer (AVC) as a viscosity modifier (2 wt%) (Figure 2h–j and Figure S2 (Supporting Information)). These gel precursors have zero-shear viscosities ranging from ≈60 to 370 Pa s, yield stresses ranging from ≈15 to 75 Pa, and storage moduli at the linear viscoelastic region ranging from ≈90 to 330 Pa (Table S2, Supporting Information). Their zero-shear viscosities are lower than those of the 8 wt% microgel ink, as is required to support the ink filament with high shape fidelity.[31] Similar to the sacrificial ink, the gel precursor material can be treated as a Herschel–Bulkley fluid, yielding consistency indices $\boldsymbol{K}$ of 7–25 and flow indices n of 0.4–0.5. These ranges of rheological parameters correspond well to those reported for other support materials for embedded 3D printing,[32] serving to inform the design of new gel precursor formulations suitable as support materials for the GUIDE-3DP strategy. For each cross-linking system, a bespoke set of reaction-initiator molecules was designed to diffuse across the interface between the printed ink and the support material (Table S1, Supporting Information). Specifically, for the photo-cross-linkable gel precursor support materials, the sacrificial gelatin microparticle ink was loaded with LAP (294 Da) as a photoinitiator, while Ca^{2+} (40 Da) was loaded as the small molecule for alginate, a cation-cross-linked gel precursor material. As PAAm requires both polymerization and cross-linking to occur simultaneously, the polymerization initiator ammonium persulfate (APS, 228 Da) and the cross-linker bis-acrylamide were included in the gelatin sacrificial ink and acrylamide support material, respectively. For the enzymatically cross-linked materials, the sacrificial ink was loaded with the enzyme thrombin (36 kDa) or transglutaminase (38 kDa) to induce gelation of fibrin or gelatin, respectively. Importantly, to avoid the transglutaminase-mediated cross-linking of the sacrificial ink for the gelatin support material, the sacrificial ink used was Pluronic F-127 (24 wt%) instead of gelatin microparticles. Pluronic F-127 is a thermoreversible triblock copolymer commonly used as a sacrificial hydrogel in 3D bioprinting applications.[21,23,33–35]

Both the inner and outer shell diameters of GUIDE-3DP channels are highly tunable, since the inner diameter is the same as the diameter of the printed sacrificial ink filament, and the outer shell diameter is dependent on the diffusion time (**Figure 3**). GUIDE-3DP offers two strategies for dynamically varying the ink filament diameters during direct writing. In one strategy, the applied dosing pressure is varied while the writing speed is held constant (Figure 3a,b); in the other strategy, the applied pressure is held constant while the writing speed is varied (Figure 3c). In both cases, the diameter of the printed ink filament dictates the inner diameter of the cross-linked GelMA tubes. The ability to control the inner diameter with the GUIDE-3DP strategy enables facile fabrication of biologically inspired, complex perfusable structures. For example, many perfusable structures in nature have inner diameters that are not constant, which can be replicated using the GUIDE-3DP strategy. As a demonstration, we created a model of the large intestine, which has a single lumen that is segmented into "pouch-like" haustra (Figure 3d), by alternating the print speed of the sacrificial ink (1 mm s^{-1}, 40 psi for an inner diameter of 4.5 mm; 2 mm s^{-1}, 40 psi for an inner diameter of 3.5 mm). As a second demonstration, we printed a perfusable network with both diverging and converging vessel branch points that emulate the natural branching observed in vascular networks in vivo, with parent vessels of larger inner diameter (2.5 mm) and daughter vessels of smaller inner diameter (1.5 mm) (Figure 3e). Upon gelatin melting and extraction of the fabricated GelMA structures, both the large intestine model and the vascular network model were readily perfusable with dye.

While the inner diameter of GUIDE-3DP channels is controlled through parameters during the printing process (i.e., applied pressure and speed), the outer diameter of the channel shell is controlled by the diffusion time after printing, during which the reaction-initiators diffuse away from the sacrificial ink into the surrounding gel precursor support material. With increasing diffusion time into the support material, the reaction-initiator is able to reach a farther distance away from the sacrificial ink, thus increasing the thickness of the outer shell (Figure 3f,g and Figure S3a–c (Supporting Information)). In the case of photo-cross-linkable gel precursors, cross-linking is terminated by turning off the UV light source; the resulting shell thickness is governed by the total distance that the reaction-initiators diffuse before termination of photo-cross-linking. In the case of thrombin-induced fibrin cross-linking and Ca^{2+}-induced alginate cross-linking, the cross-linking reactions are terminated by extracting the prints and immersing in saline buffer to remove uncross-linked material. In all cases, the relationship between the postprinting diffusion time and outer shell thickness is dependent on the diffusion rate of the reaction-initiator within the gel precursor support material, which can be modeled as Fickian diffusion. The diffusion rate can be predicted by estimating the diffusivity of the reaction-initiator through the support material. Here, we demonstrate examples for three different gel precursor materials and cross-linking approaches: GelMA as a photo-cross-linked material (reaction-initiator: LAP), alginate as a small molecule cross-linked material (reaction-initiator: Ca^{2+}), and fibrin as an enzymatically cross-linked material (reaction-initiator: thrombin). Fluorescence recovery after photobleaching (FRAP) measurements on solutes of different molecular weights (ranging between 0.7 and 250 kDa) were used to estimate the diffusivity for the corresponding reaction-initiators (Figure 3h and Figure S3d (Supporting Information)). For reaction-initiators with lower molecular weights (MWs), the higher diffusivity allows the reaction-initiator to diffuse faster (e.g., Ca^{2+} for alginate cross-linking, MW = 40 Da, $D_{est} \approx 800\ \mu m^2\ s^{-1}$, vs thrombin for fibrin cross-linking, MW = 36 kDa, $D_{est} \approx 4\ \mu m^2\ s^{-1}$). This leads to a faster rate of outer diameter increase for high-diffusivity material systems (i.e., Ca^{2+}/alginate) compared to low-diffusivity systems (i.e., thrombin/fibrin) (Figure 3g).

For a given support material/reaction-initiator combination, the Fickian diffusion of the reaction-initiator over time can be

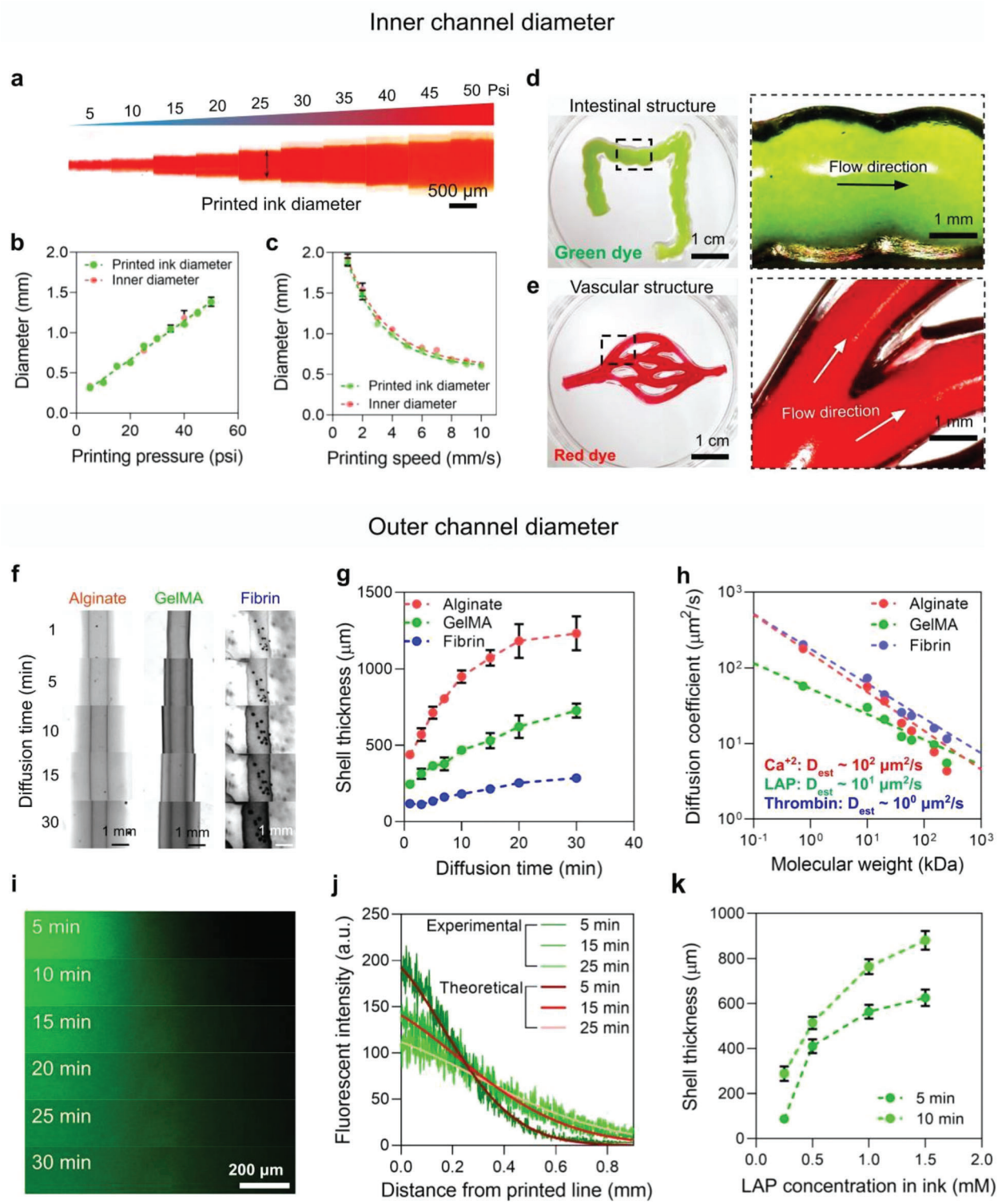

Figure 3. The inner and outer diameters of channels printed with GUIDE-3DP can be independently tuned. a) The diameter of printed inks increases with the application of greater pressure during extrusion, demonstrated between 5 and 50 psi. The inner diameter of the cross-linked channel corresponds to the diameter of the printed ink filament, which can be controlled b) as a function of applied pressure (demonstrated at a constant printing speed of 5 mm s^{-1}) and c) as a function of printing speed (demonstrated at a constant applied pressure of 25 psi). d) An intestinal model of the haustra structure was printed by adjusting the printing speed alternately between 1 and 2 mm s^{-1}. In this way, the inner diameter of the channel undulated between 4.5 and 3.5 mm. Green dye was perfused inside the cross-linked print without any leakage. e) Vascular-like networks with branch points can connect channels with varying inner diameters, with both parent (2.5 mm diameter) and daughter (1.5 mm diameter) vessels. Red dye was perfused inside the cross-linked print without any leakage. f) Brightfield microscopy images of alginate, GelMA, and fibrin channels and g) their outer shell thickness as a function of

monitored and predicted with finite element modeling (FEM). Specifically, we employed FEM to study the diffusion of LAP (MW = 294 Da, $D_{est} \approx 80$ μm^2 s^{-1}) through a GelMA gel precursor material. By first using fluorescent dextran (fluorescein isothiocyanate (FITC)–dextran, MW = 1000 Da) as a tracer molecule in the GelMA gel precursor material, we measured the experimental diffusion rate away from the printed sacrificial ink filament (Figure 3i). These measurements exhibited excellent agreement with the computational predictions (Figure 3j) using the diffusion coefficient obtained from experimental FRAP analysis (Figure 3h). Finally, in addition to the diffusion time, one can also control the diffusion rate, and hence the outer shell diameter, by simply changing the concentration of the reaction-initiator in the sacrificial ink. With higher concentrations of LAP encapsulated in the sacrificial ink (tested between 0.25 and 1.5 mM LAP), the outer GelMA shell diameter at a given time point increases (Figure 3k). With these strategies, both the inner channel diameter and the outer shell diameter of the GUIDE-3DP channels can be independently controlled.

Of the three demonstrated cross-linking approaches for solidifying the channel into a robust gel, photo-cross-linking requires a light-initiation step to induce the reaction, effectively decoupling the diffusion and reaction steps and allowing fabrication of more complex structures (**Figure 4**). This triggered cross-linking strategy is especially useful for the fabrication of branched structures with connectivity. As a first example, we demonstrate the ability to control the intersection of two GelMA channels (Figure S5a (Supporting Information) and Figure 4a). By printing two LAP-containing sacrificial ink filaments that contact each other within a GelMA support material, a continuously smooth interface is created. Following UV exposure, this results in the fabrication of a branched network with an open, seamless, leakproof interface (Figure S5a, Supporting Information). Fabricating these types of freestanding, intersecting channel structures has previously proved difficult with other technologies.[36,37]

Furthermore, we can design open networks in which different branches have unique, user-specified diameters. As described above, two strategies can be used to control the outer diameter of printed GUIDE-3DP channels: varying reaction-initiator concentrations or diffusion times (Figure 3f–k). To demonstrate how these strategies can be employed in a more complex structure, we varied the concentrations of photoinitiator within different, connected ink filaments. By modeling the photoinitiator diffusion (Figure 4a, panel i), the concentrations required to achieve the desired outer channel diameters can be determined. In this way, connected channels of different channel thicknesses (160 μm for the top branch with 1.0 mM LAP; 40 μm for the bottom branch with 0.25 mM LAP) are constructed (Figure 4a, panel ii). This type of structure (i.e., varied channel diameters connected at an open branch point) can also be achieved with a complementary approach in which the diffusion time of the photoinitiator from the ink is varied. This diffusion time control can be achieved by designing the predefined print path so that different portions of the structure are printed at precise time intervals, leading to a specified difference in diffusion time and a corresponding difference in shell thickness for different portions of the structure. In this demonstration, one filament (bottom) is printed 17 min after the first filament (top), such that the photoinitiator in the first filament has had more time to diffuse out, leading to a thicker channel (160 μm for the top branch with 20 min LAP diffusion time; 35 μm for the bottom branch with 3 min LAP diffusion time) (Figure 4b). The ability to fabricate these perfusable networks with open branch points and bespoke channel sizes is uniquely enabled by material systems in which the diffusion and reaction processes are decoupled, demonstrated here with GelMA/LAP as an exemplary photo-cross-linkable material.

Furthermore, GUIDE-3DP allows for increased design complexity via the fabrication of multilumen structures. When two neighboring, parallel lines are printed, they can either fuse to form a single bulk structure with two internal channels or remain as two distinct, separate channels depending on the overlapping diffusion profiles of the reaction-initiator (Figure S5b, Supporting Information). The reaction-initiator spatial profile can be predicted using finite element modeling of adjacent filaments (Figure S5b, panel ii, Supporting Information). Specifically, the fabrication of cohesive, fused channels is facilitated by shorter distances between the printed lines and longer diffusion times (Figure 4c). These predictions allow for the design of multiple perfusable networks fused into a cohesive structure, which may be advantageous when fabricating complex constructs that require manipulation (e.g., for implantation) due to the increased structural rigidity.

Having established these physical principles of GUIDE-3DP with photoactive cross-linkers (Figure 4a–c), we next sought to demonstrate fabrication of physiologically relevant structures. As a first example, we selected a model of the human coronary sinus and cardiac veins, which have differing internal and outer diameters (Figure 4d, panel i).[38,39] COMSOL modeling of LAP diffusion through GelMA informed the diffusion time required to fabricate these branched channels of the desired geometry (Figure 4d, panels ii and iii). The creation of this tubular architecture with open intersections of multiple smaller channels was validated with a GelMA print, which had sufficient structural integrity to be removed from the support material for imaging (Figure 4e).

Using the GUIDE-3DP strategy with photo-cross-linkable materials also allows us to design two or more distinct perfusable networks within the same structure (Figure S5c (Supporting Information) and Figure 4f). This is enabled by formulating the sacrificial ink to be thixotropic and self-healing, which allows the nozzle to pass through the printed path of the first network without causing permanent deformation while printing the path of the second network. In this way, two intertwined perfusable channels were fabricated, opening the door to printing of more complex vascular-like networks, which often require the extrusion

diffusion time. h) FRAP analysis for freely diffusing fluorescent dextrans of varying molecular weights (0.7–250 kDa) in alginate, GelMA, and fibrin gel precursor support materials. i) Confocal microscopy images of a fluorescent dextran (FITC–dextran, MW = 10 kDa) diffusing from a single printed filament in a GelMA support material as a function of diffusion time. j) Experimental measurements of diffusion are in close agreement with simulation results of predicted diffusion obtained with finite element analysis. k) GelMA shell thickness is dependent on the concentration of the reaction-initiator (LAP) in the sacrificial ink.

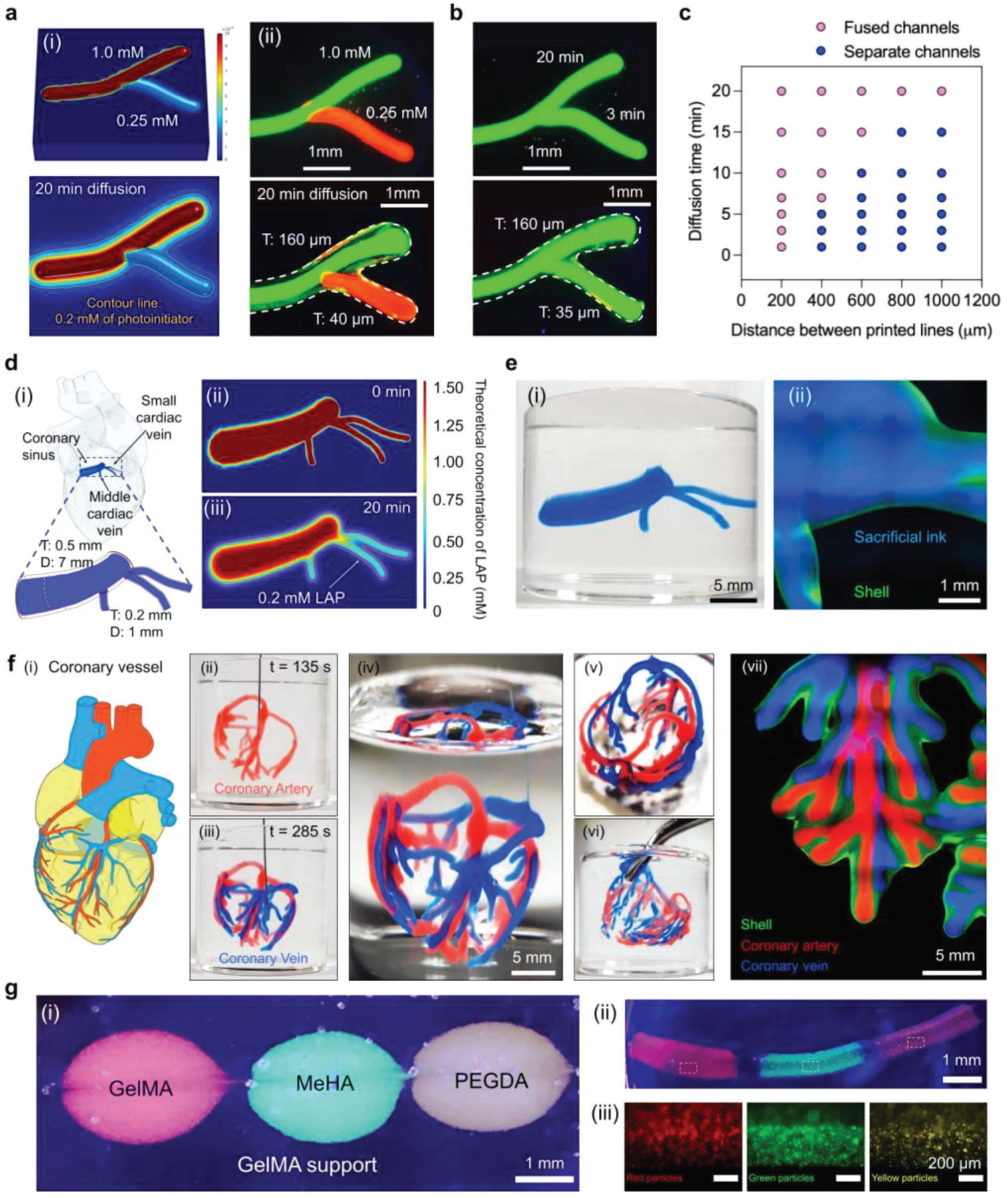

Figure 4. Complex perfusable networks are fabricated with the GUIDE-3DP method. a) i) A computational model of a bifurcated channel predicts LAP diffusion into GelMA for a structure using two sacrificial inks with different LAP concentrations. ii) GUIDE-3DP printing of the model in (i) confirmed fabrication of channels with differing shell thickness connected at an open branch point. b) Fabrication of channels with differing shell thickness is also achieved by controlling the LAP diffusion time from a single sacrificial ink. c) Neighboring, parallel channels can either fuse together to form a single bulk structure with two internal channels or remain as two distinct, separate channels. d) Construction of a print mimicking the coronary sinus connected

nozzle to pass through ink that has been previously deposited (Figure S5c, Supporting Information).

As a prerequisite for a functional vascular network, the perfusable nature of fabricated structures was further demonstrated using particle image velocimetry (PIV) (Figure S5d,e , panel i and Videos S1 and S2, Supporting Information) coupled with finite element modeling (Figure S5d,e, panel ii, Supporting Information). The fluid dynamics within printed structures are highly tunable and predictable, as demonstrated by the different flow profiles within straight channels at various flow rates and within branched channels at various locations (Figure S5d,e, panel iii, Supporting Information).

As a demonstration, we printed a coronary vascular network geometry within a GelMA support using cardiac structural data from the National Institutes of Health 3D Print Exchange (Figure 4f). This coronary vessel structure was built by first printing the coronary artery structure (red ink) and then the coronary vein structure (blue ink) (Figure 4f, panels ii and iii). Both coronary structures were stable during printing and exhibited no visible changes after UV cross-linking. Cross-linking was performed 20 min after finishing the printing process, demonstrating the short working times achievable with our GUIDE-3DP method (Figure 4f, panels iv and v). The coronary-vessel-like print demonstrated high structural integrity, allowing it to be removed from the un-cross-linked gel precursor support material with forceps for rinsing with saline (Figure 4f, panel vi). The resulting structure is sufficiently stable and self-supporting so that it can be easily picked up, handled, and transferred. Confocal microscopy images show that the UV-cross-linked shell structures stained by FITC–dextran homogeneously surround the printed vessels (Figure 4f, panel vii). We observed excellent extrusion consistency and structural stability throughout the 3D printing process, which was evident from the high lateral and axial uniformity observed across the coronary artery and coronary vein structures. This excellent shape fidelity was not only reflected by the overall design, but also by the self-supporting nature of the single branches and furcated vessels, which did not show any sagging at elevated temperatures. For such complex structures, the sequence by which branches are printed is crucial, as these more time-consuming prints will experience a range in diffusion time between the first and last structures to be printed. To account for and leverage this variation, we printed the thicker, parent vessels in each structure first and the thinner, daughter vessels afterward, for a total print time of 285 s. In the future, triggered release systems could be developed to exert greater control over the timing of reaction-initiator diffusion. Alternatively, multinozzle printers could be developed to minimize the total printing time.

From these examples, we show that the GUIDE-3DP process is highly tunable: the inner diameter of printed structures primarily depends on the nozzle size, extrusion rate, and print speed, with lumen diameters of 300 μm to 2 mm being achieved in this study using a 27-G needle (Figure 3a–c). To fabricate channels with larger diameters (>5 mm), multiple parallel filaments can be fused to increase the dimensions (Figure 4d,e). The outer diameter can be freely adjusted (here, we demonstrate shell thickness ranging from 100 to 1200 μm) based on the diffusion kinetics, selection of precursor material system, reaction-initiator concentration, and time allowed for diffusion before termination of cross-linking (Figure 3f,g).

With the GUIDE-3DP strategy, different materials that utilize the same reaction-initiator may also be cross-linked together into a cohesive print. As a demonstration, we fabricated three photo-cross-linkable materials into a single, perfusable structure (Figure 4g). Prelabeled GelMA, MeHA, and PEGDA were first 3D printed into distinct regions within a larger, unlabeled GelMA support matrix; then upon printing a single, LAP-containing sacrificial ink, a continuous channel with different material segments was formed.

As an additional advantage, all material combinations shown in this study enable the entire fabrication process to be conducted at room temperature without additional temperature control. For GelMA, this is enabled by synthesizing the gel precursor support material from cold-water-fish-skin-derived gelatin, resulting in a polymer with stable rheological properties across a temperature range of 25–40 °C (Figure S4a, Supporting Information).

By varying the gel precursor material compositions and reaction-initiator concentrations, the mechanical properties of fabricated structures can be readily tuned. For example, we demonstrate that by varying the GelMA concentrations in the gel precursor support material, the shear moduli of cross-linked channel materials span ≈1 to ≈80 kPa (Figure S4b,c, Supporting Information). Furthermore, the final mechanical properties of cross-linked channel materials will depend on the reaction-initiator concentration, which may translate to a gradient in stiffness along the thickness of printed channels; this effect is more pronounced for GelMA than for alginate or fibrin (Figure S4d,e, Supporting Information). The localized stiffness along the length of a print may also be dependent on the print path, which determines the proximity of a given region to other filaments and thus the local reaction-initiator concentration. For instance, regions near branch points may exhibit higher concentrations of reaction-initiator, resulting in greater stiffnesses which serve to reinforce the structure. As a result, a variety of parameters, including the material type and composition, reaction-initiator concentration, and print path design, can be tuned to modulate both the local and bulk mechanical properties of a printed structure.

Besides their tunable mechanical properties, another important characteristic of printed structures is their mechanical stability over time. We show that GelMA and fibrin channels exhibit a stable stiffness over 7 days at 37 °C in endothelial growth

to small and middle cardiac veins (panel i). The theoretical concentration of LAP initially (panel ii) and 20 min after 3D printing (panel iii). e) Photo of printed coronary sinus and cardiac veins (panel i) and close-up fluorescence microscopy image (panel ii) showing the GelMA shell (green) and sacrificial ink (blue). f) To fabricate a model of the coronary vessels (panel i), the artery and vein networks were printed sequentially (panels ii and iii). Side and top views of the printed coronary vessel structure (panels iv and v). The printed coronary vessel structure can be picked up with forceps (panel vi). Close-up fluorescence microscopy image showing the GelMA shell (green) around the arterial network (red) and the venous network (blue) (panel vii). g) Multiple photo-cross-linkable materials (GelMA, MeHA, and PEGDA) can be fabricated into a single channel structure using a print-in-print method. Individual regions of labeled GelMA (red), MeHA (green), and PEGDA (yellow) are first printed within a GelMA support material (panel i). All three gel precursors are cross-linked with the same reaction-initiator (LAP) to form a continuous channel (panels ii and iii).

medium-2 (EGM-2) cell culture medium. While alginate channels were found to exhibit a loss in stability in EGM-2 alone, they were able to retain their stiffness in EGM-2 supplemented with 250 mM Ca^{2+} (Figure S4f, Supporting Information). This result is to be expected, since monovalent ions in cell culture medium compete with divalent ions for the binding sites on the α-L-guluronic acid monomers of alginate, leading to a loss of mechanical properties over time.[40] With supplementation of Ca^{2+}, the exchange of Ca^{2+} within the printed structure with monovalent ions is reduced, enabling the mechanical stability of alginate channels during culture.

Finally, the GUIDE-3DP strategy allows for not only fabrication of channels with biologically relevant geometries but also integration with living cells, as the hydrogel materials used in this study are highly cytocompatible.[41–43] We demonstrate the cytocompatibility of our material system by seeding human umbilical vein endothelial cells (HUVECs) on GelMA-based channel materials. As fibronectin and fibrinogen are known to enhance cellular adhesion in vitro,[44,45] we incorporated 0.05 wt% fibronectin or 2.5 wt% fibrinogen into the GelMA-based gel precursor support material, each of which also contained 2.5 wt% of the viscosity enhancer Aristoflex AVC. Cells seeded on cross-linked GelMA, GelMA–fibronectin, and GelMA–fibrinogen materials exhibited high viability (>90%) 3 days after seeding (Figure S6a–c, Supporting Information). As expected, the number of adherent cells increased for GelMA–fibronectin and GelMA–fibrinogen compared to GelMA (Figure S6a,b, Supporting Information), and these two formulations sustained high viability (>90%) 7 days after seeding (Figure S6a–c, Supporting Information). Furthermore, HUVEC on GelMA–fibronectin and GelMA–fibrinogen maintained their endothelial phenotype, as evidenced by expression of vascular endothelial (VE)-cadherin and cluster of differentiation 31 (CD31) (Figure S6d, Supporting Information). Between these two formulations, a higher cell density (and hence greater confluency) was achieved on GelMA–fibrinogen, while increased cell spreading was achieved on GelMA–fibronectin (Figure S6e,f, Supporting Information). Owing to the demonstrated cytocompatibility of hydrogel materials, tailored vessel structures can be seeded with HUVECs to achieve an in vitro cell-lined blood vessel model. Customizable vessels with tunable dimensions and multiple furcation points are highly relevant as models for stenosis or vessel calcification.[46,47]

Successful seeding of HUVECs was demonstrated within GelMA channels fabricated with GUIDE-3DP (**Figure 5**). The HUVECs were injected into the hollow channels, and adherent cells showed high cell viability 3 days after seeding (Figure 5a,b), with the vast majority of the cells attaching to the inner lumen of the channel and a few cells attaching to the outer surface of the vessel shell. As a demonstration of a more complex vasculature-like structure, we fabricated a branched channel network (Figure 5c). The channel, which consisted of a thicker parent vessel (inner diameter: 2 mm) with four smaller daughter vessels (inner diameters: 1.0–1.5 mm), showed a continuously open lumen that was fully perfusable without leakage (Figure 5c, panel i). Therefore, the lining of the vessel lumen with viable HUVECs was possible (Figure 5c, panels ii–iv).

Based on the enhanced cell adhesion demonstrated on GelMA–fibronectin materials (Figure S6, Supporting Information), we incorporated 0.05 wt% fibronectin within the GelMA gel precursor support material prior to printing to demonstrate versatility in the biochemistry of GUIDE-3DP structures. While the viability of HUVECs was similar (around 70% live cells) for seeding within GelMA-only or GelMA–fibronectin prints (Figure S7, Supporting Information), the HUVECs exhibited greater spreading and expression of the endothelial adhesion molecule VE-cadherin along the inner lumens of GelMA–fibronectin channels (Figure S8, Supporting Information). The enhanced cellular spreading due to the added fibronectin is demonstrated by the increased overall cytoskeletal area per cell (261 ± 127 μm^2 for GelMA–fibronectin vs 135 ± 84 μm^2 for GelMA-only). Additionally, we show that other biomolecules, such as fibrinogen, can similarly be incorporated into the GelMA-based support material to enhance cell adhesion. HUVEC maintained high viability (≈85%) within GelMA–fibrinogen channels 3 and 7 days postseeding (Figure S7b,e, Supporting Information), along with a phenotypic spread morphology and expression of VE-cadherin at cell junctions 7 days postseeding (Figure S8c,d, Supporting Information). These results demonstrate the sustained maintenance of HUVEC within these fabricated tubular structures. Thus, the GUIDE-3DP strategy allows for the integration of complex, branching, perfusable channels with living cells and is amenable to the addition of biomolecules in the gel precursor support material for future optimization of cell function.

3. Conclusion

We report a new 3D printing strategy termed GUIDE-3DP for fabricating bespoke, perfusable networks of self-supporting, interconnected channels. To achieve user-specified channel dimensions, this technique leverages the predictable diffusion of reaction-initiators released from sacrificial inks printed within the hydrogel precursor. The inner and outer diameters of vessels can be independently varied within a single print: inner diameters are controlled by the printing pressure and speed, while outer diameters are controlled by the reaction-initiator concentration and diffusion time. Finite element modeling can be used to relate the desired dimensions of a channel network to the printing parameters. Importantly, multiple channels can be seamlessly connected at branch points, and multiple networks of channels can be integrated into a single, cohesive, self-supporting print. We created a library of seven hydrogel precursor materials (gelled via photo-cross-linking, small molecule cross-linking, or enzymatic cross-linking) and their corresponding reaction-initiators to highlight the versatility of this technology. Finally, we demonstrated the integration of the GUIDE-3DP approach with living endothelial cells that lined the inner lumens of blood-vessel-like channels. Altogether, this technology represents an important advance toward the fabrication of self-supporting, physiologically relevant networks with intricate and perfusable geometries.

4. Experimental Section

Gel Precursor Support Material Preparation: For the GelMA gel precursor material, GelMA was synthesized using a protocol similar to those described previously.[48] Gelatin from cold water fish skin (Sigma-Aldrich) was dissolved at 20 wt% in 0.1 M carbonate–bicarbonate buffer at 37 °C overnight. The pH was adjusted to 10. Methacrylic anhydride (MAA, 94%,

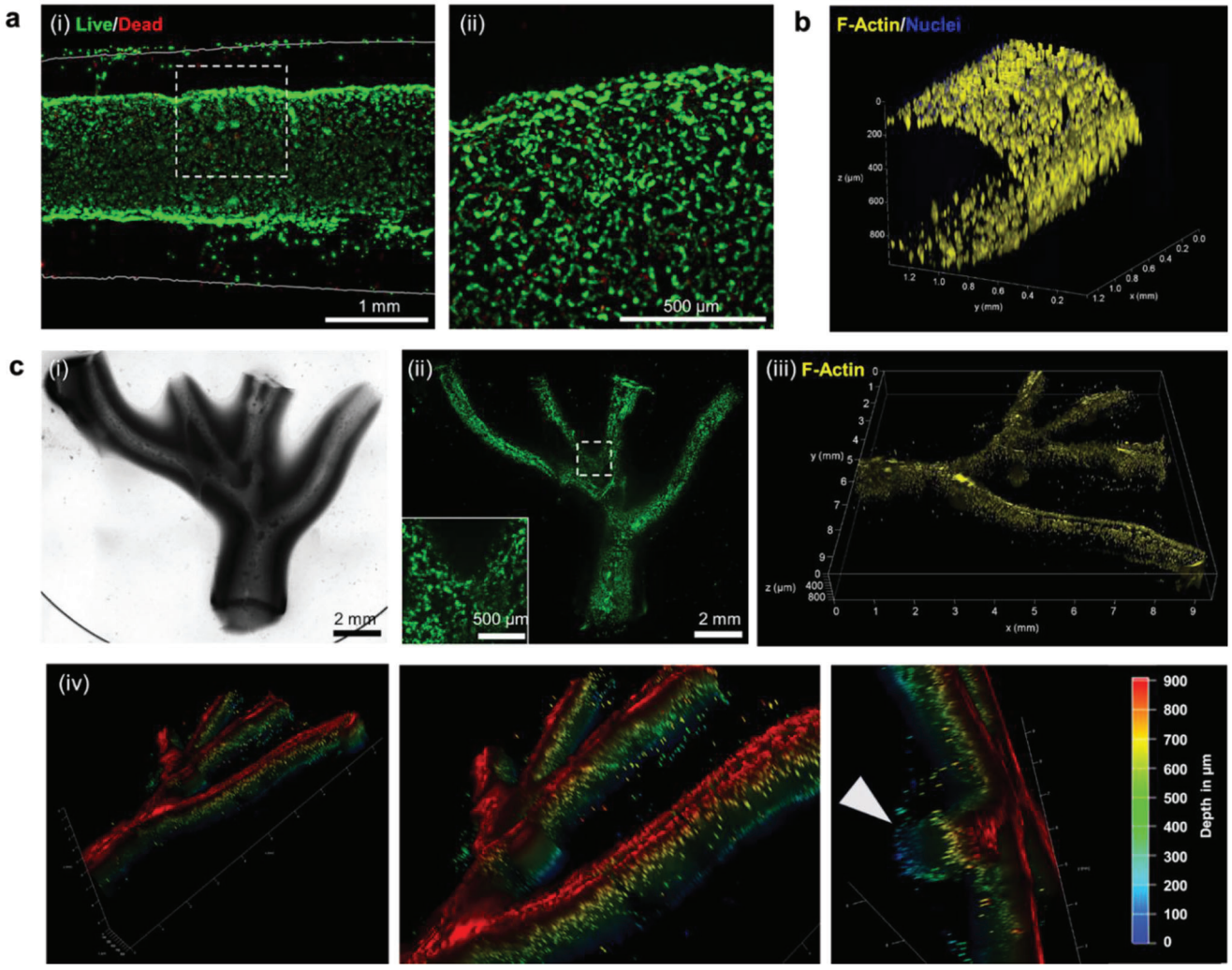

Figure 5. The inner lumens of perfusable vessels printed with GUIDE-3DP can be seeded with endothelial cells. a) Representative fluorescence images of a GelMA channel 3 days postseeding: i) image of viable (green, calcein AM) and dead (red, ethidium homodimer-1) HUVECs within the inner lumen (diameter = 2 mm), with the outer vessel wall (thickness = 1 mm) indicated by the solid gray lines; ii) magnified view of cells at the vessel wall interface, with the acquisition position indicated by the dashed white box in (i). b) 3D reconstruction of the HUVEC-lined vessel stained for F-actin cytoskeleton (yellow) and nuclei (blue). c) Representative images of a HUVEC-lined, furcated GelMA structure: i) brightfield image; ii) fluorescence image of viable HUVECs (green, calcein AM) and (inset) magnified view at a channel furcation point; iii) 3D reconstruction of the furcated channel network stained for F-actin (yellow); and iv) depth-coded images with white arrow indicating the patent, circular vessel lumen.

Sigma-Aldrich; 83 µL g^{-1} of gelatin) was added dropwise while stirring at 100–200 rpm. The reaction was allowed to proceed at 70 °C for 2 h. GelMA was precipitated and collected after pouring the reaction mixture into ≈3× reaction volume of ethanol. After drying the GelMA (>24 h), it was dissolved in deionized (DI) water at ≈80 °C for at least 1 h while stirring to remove residual ethanol. The GelMA concentration was determined as percentage of dry mass. To prepare the support material, respective stock solutions of GelMA and Aristoflex AVC (Lotioncrafter) were blended to achieve the desired final concentrations.

For the PEGDA support material, 10 wt% of PEGDA, MW: 20 kDa was dissolved in phosphate-buffered saline (PBS). The 10 wt% PEGDA solution was mixed in a 1:1 ratio with a 4 wt% AVC stock solution to form the 5 wt% PEGDA + 2 wt% AVC support material.

For the MeHA support material, sodium hyaluronic acid (Lifecore Biomedical, 40 kDa MW) was dissolved in deionized water at 1 wt%. MAA (94%, Sigma-Aldrich) was slowly added to the solution. The pH was adjusted to 8–9 with sodium hydroxide solution (6 N) and the solution was gently stirred at 4 °C for 18 h, protected from light. The MeHA was subsequently precipitated by ethanol (95%) and dialyzed against deionized water using a cellulose acetate tube (molecular weight cutoff: 12 kDa) for three days, followed by lyophilization. The 2 wt% MeHA solution was then mixed in a 1:1 ratio with a 4 wt% AVC stock solution to form the 1 wt% MeHA + 2 wt% AVC support material.

For the PAAm support material, 40 wt% of acrylamide (Sigma-Aldrich) and 0.2 wt% of *N*,*N*′-methylenebis(acrylamide) (Sigma-Aldrich) were dissolved in deionized water. They were mixed with a 4 wt% AVC stock solution to form the 20 wt% acrylamide + 0.1 wt% *N*,*N*′-methylenebis(acrylamide) + 2 wt% AVC support material.

For the alginate support material, alginic acid sodium salt from brown algae (Sigma-Aldrich) was dissolved at a concentration of 4 wt% in PBS. The 4 wt% alginate solution was then mixed in a 1:1 ratio with a 4 wt% AVC stock solution to form the 2 wt% alginate + 2 wt% AVC support material.

For the fibrin support material, bovine fibrinogen (MP Biomedicals) was dissolved at a concentration of 10 wt% in PBS, and then mixed with a 4

wt% AVC stock solution to form the 5 wt% fibrinogen + 2 wt% AVC support material.

For the gelatin support material, gelatin from cold water fish skin (Sigma-Aldrich) was dissolved at 20 wt% in PBS, and then mixed with a 4 wt% AVC stock solution to form the 10 wt% gelatin + 2 wt% AVC support material.

Sacrificial Ink Preparation: To prepare the gelatin microparticle ink used in acellular printing experiments, gelatin microparticles were synthesized by complex coacervation, as previously described.[48] Briefly, a solution of 6.4 wt% gelatin type A (300 bloom, Sigma-Aldrich), 0.5 wt% Pluronic F-127 (Sigma-Aldrich), and 0.2 wt% gum arabic (Alfa Aesar) in DI water was heated in a microwave until bubbling. Ethanol was added at 1 mL g^{-1} of gelatin solution while stirring at 500 rpm. The mixture was then stirred overnight at 500 rpm at room temperature. The gelatin microparticles were collected and washed 3 times with DI water using a Büchner funnel, and the resultant slurry was compacted via vacuum filtration. The concentration of microparticles in the jammed slurry was determined as the percent dry mass after drying aliquots in a vacuum oven for 2 h at 60 °C. Prior to printing, the microparticle concentration was adjusted to 4–10 wt% using a solution of reaction-initiator in PBS (or Hank's Balanced Salt Solution, HBSS, for an alginate support material) such that the desired reaction-initiator concentration was achieved (Table S3, Supporting Information). The reaction-initiators included in the inks were calcium chloride dihydrate (Millipore) for an alginate support material, APS (Sigma-Aldrich) for a PAAm support material, bovine thrombin (MP Biomedicals) for a fibrin support material, and LAP (Sigma-Aldrich) for GelMA, MeHA, and PEGDA support materials. For cellular printing experiments, sterile lyophilized gelatin microparticles (LifeSupport, FluidForm Inc.) were rehydrated at a concentration of 10 wt% in sterile, cold PBS containing 5 mM LAP. For the gelatin support material, a sacrificial ink of 24 wt% Pluronic F-127 containing 1 wt% transglutaminase was used instead of gelatin microparticles.

Rheological Characterization: To measure the rheological properties of the gel precursor support materials and sacrificial ink, samples were loaded onto an ARG2 stress-controlled rheometer (TA Instruments) equipped with a 40 mm diameter parallel plate geometry at a 1.0 mm gap height. Samples were subjected to shear stress-sweep experiments over a stress range of 0.1–1000 Pa at a frequency of 1 Hz at 25 °C. The viscosity was measured at 25 °C using a range of shear rates from 0.1 to 1000 s^{-1}. The step-stress was measured at both a high-magnitude stress (300 Pa) and a low-magnitude stress (0.1 Pa). To characterize the temperature dependence of the gelatin microgel ink and GelMA gel precursor properties, temperature sweep experiments were performed from 25 to 37 and from 25 to 40 °C, respectively.

Mechanical Testing of Cross-Linked Hydrogels: Alginate, GelMA, and fibrin hydrogels were cross-linked with different concentrations of Ca^{2+}, LAP, and thrombin, respectively, and prepared in circular disks (8 mm diameter). A strain-controlled amplitude sweep (0.01–1% strain) at a frequency of 1 Hz with a parallel plate geometry (8 mm diameter) was used to determine the linear viscoelastic region at 25 °C. Samples were then incubated at 37 °C for 7 days in endothelial growth medium (EGM-2 BulletKit, Lonza) to evaluate their long-term stability. The shear modulus at 37 °C was measured at different time points of incubation using a strain-controlled amplitude sweep (0.01–1% strain) at a frequency of 1 Hz.

Compression testing was performed using a universal testing machine (GB/LRX Plus, Lloyd, West Sussex, UK) fitted with a 10 N load cell. For the test, cross-linked alginate, GelMA, and fibrin hydrogels were prepared in circular disks (8 mm diameter) with 2 mm thickness. Stress–strain curves under uniaxial compression were plotted for strains ranging from 0% to 60%.

FRAP: Alginate, GelMA, and fibrin support materials were prepared with FITC-labeled diffusants (either 1 μg mL^{-1} diazide–PEG–FITC or 10 μg mL^{-1} of 10, 20, 40, 60, 150, 250 kDa FITC–dextran, Sigma). 150 μL of the diffusant-laden support materials was loaded into a clear bottom, 96-well plate and centrifuged to remove bubbles. FRAP experiments were performed using a confocal microscope (Leica SPE) with 30 s of photobleaching (100 μm × 100 μm area, 488 nm laser, 100% intensity) and 90 s of capture time. Diffusion coefficients for each condition were calculated using the open source MATLAB code "frap_analysis" based on the Hankel transform method.[49]

3D Printing: 3D printing was performed with a custom-built dual-extruder bioprinter modified from a MakerGear M2 Rev E plastic 3D printer[50–52] and a custom-built pneumatic printer modified from a Creality Ender 3 3D printer.[53,54] Prior to printing, the sacrificial ink was loaded into a 2.5 mL Hamilton Gastight syringe. Support materials were added to well plates or custom-made polycarbonate containers and centrifuged at 4000 rpm for 5 min at room temperature to remove bubbles. Print paths were created using the commercially available Rhinoceros software (Rhinoceros 5.0, Robert McNeel & Associates, Seattle, WA, USA). Using the Rhinoceros software, designed printing paths (2D lines) were segmented with "divide" function to create 1D dots to determine the cartesian coordinates. The cartesian coordinates were saved as a .txt file and translated into G-code to set extrusion rates using CAMotics software. After printing, diffusion of the reaction-initiator was allowed to occur for a specified amount of time (Table S1, Supporting information). For photo-cross-linkable materials (GelMA, MeHA, and PEGDA), the printed structure was cross-linked at 365 nm for 5 min using a UV lamp. After cross-linking, the structure was removed from the un-cross-linked support material using a metal spatula and washed by gently shaking in a 50 mL conical tube containing PBS (or HBSS for an alginate support materials). Once washed, the structures were placed into fresh PBS (or HBSS), and the sacrificial ink was melted by incubating at 37 °C for gelatin microparticles or at 4 °C for Pluronic F-127. The ends of the structures were cut, either before or after sacrificial ink melting, to allow fluid perfusion.

As preparation for endothelialization, materials and channels were processed in an aseptic environment. The support materials were autoclaved prior to use. To create linear GelMA and GelMA–fibronectin channels (length = 2 cm), a 10 wt% gelatin microparticle ink containing 5 mM LAP was printed into a 20 wt% GelMA + 2.5 wt% AVC support material with and without 0.05 wt% fibronectin. To create the branched structure (total size $x = 13.7$ mm, $y = 11.7$ mm), the same sacrificial ink was printed into a 20 wt% GelMA + 2.5 wt% AVC support material. To fabricate GelMA–fibrinogen channels, a 10 wt% gelatin microparticle ink containing 5 mM LAP and 500 U mL^{-1} thrombin was printed into a 10 wt% GelMA + 2.5 wt% AVC + 2.5 wt% fibrinogen support material. After printing, the ends of the channels were cut using a sterile scalpel to enable subsequent perfusion seeding. Vessels were incubated in sterile PBS for at least 24 h at 37 °C prior to endothelialization.

Cell Culture and Endothelialization of Printed Structures: HUVECs (PromoCell) were expanded to passage 6 or 7 in endothelial growth media (EGM-2 BulletKit, Lonza), and culture medium was changed every other day. For cell seeding on the inner lumen of 3D printed channels, HUVECs were enzymatically detached in 0.025% Trypsin–ethylenediaminetetraacetic acid (Gibco) for 5 min at 37 °C and resuspended in EGM-2 media at $\approx 1 \times 10^7$ cells mL^{-1}. The cell suspension was then injected via pipette into the vessel lumen (≈20 μL ≙ 2×10^5 cells cm^{-1} of vessel length). The channels were incubated at 37 °C for a total of 80 min, during which two incubation steps were performed on each side, flipping by 180° and injecting 20 μL of fresh cell suspension between each step, to allow HUVEC adhesion to the entire inner lumen. Vessels were incubated in EGM-2 medium after cell seeding, and culture medium was changed every other day.

Perfusion and Investigation of Fluid Flow: To characterize the fluid dynamics within printed structures, printed structures were perfused with PBS containing 0.1 wt% fluorescent beads using a syringe pump at flow rates ranging from 0.1 to 1 mL h^{-1}. Particle image velocimetry was performed using a frame rate of 30 pictures s^{-1}, and flow profiles were determined using the MATLAB PIVlab tool (version 2.62.0.0). A Gaussian filter was applied to each image, and the average background noise was subtracted from the images. The velocity vectors were obtained by applying 2D cross-correlations of the interrogation windows of sizes 128 × 128 pixels with 50% overlap for the coarse grid and 64 × 64 pixels with 50% overlap for the refined grid system.

Cell Viability Assay: To characterize the cytocompatibility of support materials, hydrogels consisting of 20 wt% GelMA + 2.5 wt% AVC with and without 0.05 wt% fibronectin, as well as 10 wt% GelMA + 2.5 wt% AVC

with 2.5 wt% fibrinogen, were prepared in 24-well plates and cross-linked using a UV lamp. A cell suspension of 1.5×10^5 cells mL^{-1} was prepared, and 1 mL was seeded onto each gel for a final seeding density of 8×10^4 cells cm^{-2}. Culture medium was changed every other day thereafter.

Cell viability on cross-linked GelMA hydrogels and 3D printed structures was assessed using Live/Dead staining (Thermo Fisher Scientific). Live cells were stained with calcein AM (2 µM) and dead cells were stained with ethidium homodimer-1 (EthD-1; 4 µM) in PBS for 30 min at 37 °C. Fluorescence microscopy was performed using a Leica THUNDER fluorescence microscope. Images of cross-linked GelMA hydrogels and Z-stack images (total thickness 800–1000 µm) of 3D printed structures were processed in Fiji (version 1.53).[55] Cell viability was calculated as the ratio (in %) of viable cells (calcein-AM-stained cells) to all cells (sum of calcein-AM- and EthD-1-stained cells).

Immunostaining and Imaging: For immunocytochemistry to observe cell distribution and morphology, samples were fixed for 30 min using 4% paraformaldehyde in PBS, then washed 3 times with PBS for 15 min each. Cells were permeabilized with 0.1% Triton X-100 in PBS (PBST) for 1 h. Nonspecific binding was prevented by blocking in 0.05% Triton X-100, 5% normal goat serum, and 0.5 wt% bovine serum albumin (BSA, Roche) in PBS for 3 h. Primary antibody anti-VE-cadherin (Rabbit mAb, Cell Signaling Technology, 1:250) diluted in 0.05% Triton X-100, 2.5% normal goat serum, and 0.25 wt% BSA was applied for 1 h at room temperature, followed by four washing steps in PBS for 20 min each. A fluorescently tagged secondary antibody (Goat anti-rabbit, Alexa Fluor 647, Thermo Fisher Scientific) diluted in the same antibody solution was applied for 1 h, followed by three PBS washes for 20 min. For cells seeded on cross-linked GelMA hydrogels, an additional primary antibody, anti-CD31 (Mouse mAb, Abcam, 1:200), was included, along with an additional fluorescently tagged secondary antibody (Goat anti-mouse, Alexa Fluor 488, Thermo Fisher Scientific) in the secondary antibody step. Cell nuclei and actin cytoskeleton were stained by incubation with 4′,6-diamidino-2-phenylindole, dihydrochloride (Thermo Fisher Scientific, 1 µg mL^{-1}) and phalloidin–tetramethylrhodamine B isothiocyanate (Sigma-Aldrich, 0.2 µg mL^{-1}) in PBST for 1 h at room temperature, followed by three PBS washing steps for 15 min. Printed structures were imaged using a Leica THUNDER fluorescence microscope, and cross-linked hydrogels were imaged using a Leica STELLARIS 5 confocal microscope. Cell size and density were quantified using CellProfiler (version 4.2.5), and representative images were processed using Fiji (version 1.53).

Computational Modeling of Photoinitiator Diffusion: COMSOL Multiphysics (version 5.6) was employed to simulate the diffusion of the photoinitiator LAP from the printed sacrificial ink filament over time. A 3D finite element model was created using a time-dependent study in the transport of diluted species interface. The model geometry was imported with a stereolithography (STL) file designed according to the G-code path, and the diameter was set according to that of the printed filament. To simulate LAP transport, the diffusion coefficient of LAP obtained using FRAP ($D_{est} \approx 80\ \mu m^2\ s^{-1}$) was entered into the model, and the initial concentration of LAP in the sacrificial ink was set according to experimental values. A tetrahedral physics-controlled mesh with the predefined finer element size was used in all simulations. The concentration profiles of LAP as a function of distance from the ink filament were then calculated for diffusion times ranging between 0 and 30 min.

Statistical Analysis: Results were plotted in GraphPad Prism (version 9.3). For comparisons of shear moduli of 3D printed channels ($n = 3$) over time, a two-way analysis of variance (ANOVA) with Tukey post-hoc test was performed. For comparisons of cell viability on cross-linked GelMA hydrogels ($n = 3$) and 3D printed channels ($n \geq 3$), statistical significance was assessed using an ordinary one-way ANOVA with Tukey post-hoc test. For comparisons of cell areas on cross-linked GelMA hydrogels and 3D printed channels, statistical significance was assessed using a two-tailed Mann–Whitney test (total cell number $n > 750$) and a Kruskal–Wallis test (total cell number $n > 500$), respectively. For the comparison of cell densities, a two-tailed unpaired t test was performed ($n = 3$). In all cases, $p < 0.05$ was considered as a statistically significant difference. Data were presented as the mean ± the standard deviation unless specified otherwise.

Supporting Information

Supporting Information is available from the Wiley Online Library or from the author.

Acknowledgements

S.C.H. acknowledges support from the National Science Foundation (Grant Nos. DMR-2103812, CBET 2033302) and the National Institutes of Health (Grant Nos. R01-EB027171, R01-HL142718, R01-HL151997). L.G.B. acknowledges support from the National Science Foundation Graduate Research Fellowship Program (Grant No. DGE-1656518). B.C. acknowledges support from the Stanford Knight-Hennessy Scholars program. J.G.R. acknowledges support from the National Science Foundation Graduate Research Fellowship Program (Grant No. DGE-1656518) and the Stanford Smith Family Graduate Fellowship.

Conflict of Interest

S.S., J.G.R., A.J.S., and S.C.H. are inventors on a nonprovisional patent application (no. 18/142931, filed 3 May 2023) related to this work, submitted by the Board of Trustees of Stanford University.

Data Availability Statement

The data that support the findings of this study are available from the corresponding author upon reasonable request.

Keywords

3D bioprinting, interfacial gelation, perfusable networks, vascular mimics

Received: June 29, 2023
Published online:

[1] E. K. Hendow, P. Guhmann, B. Wright, P. Sofokleous, N. Parmar, R. M. Day, *Fibrog. Tissue Repair* **2016**, *9*, 3.
[2] K. Ahookhosh, O. Pourmehran, H. Aminfar, M. Mohammadpourfard, M. M. Sarafraz, H. Hamishehkar, *Eur. J. Pharm. Sci.* **2020**, *145*, 105233.
[3] C. O'Connor, E. Brady, Y. Zheng, E. Moore, K. R. Stevens, *Nat. Rev. Mater.* **2022**, *7*, 702.
[4] M. Schaupper, M. Jeltsch, S. Rohringer, H. Redl, W. Holnthoner, *Tissue Eng., Part B* **2016**, *22*, 395.
[5] J. Basu, T. A. Bertram, *Toxicol. Pathol.* **2014**, *42*, 82.
[6] C. J. Mandrycky, C. C. Howard, S. G. Rayner, Y. J. Shin, Y. Zheng, *J. Mol. Cell. Cardiol.* **2021**, *159*, 1.
[7] L. Si, H. Bai, M. Rodas, W. Cao, C. Y. Oh, A. Jiang, R. Moller, D. Hoagland, K. Oishi, S. Horiuchi, S. Uhl, D. Blanco-Melo, R. A. Albrecht, W.-C. Liu, T. Jordan, B. E. Nilsson-Payant, I. Golynker, J. Frere, J. Logue, R. Haupt, M. McGrath, S. Weston, T. Zhang, R. Plebani, M. Soong, A. Nurani, S. M. Kim, D. Y. Zhu, K. H. Benam, G. Goyal, et al., *Nat. Biomed. Eng.* **2021**, *5*, 815.
[8] G. J. Mahler, M. B. Esch, R. P. Glahn, M. L. Shuler, *Biotechnol. Bioeng.* **2009**, *104*, 193.
[9] M. Carrabba, P. Madeddu, *Front. Bioeng. Biotechnol.* **2018**, *6*, 41.
[10] L. Gui, L. E. Niklason, *Curr. Opin. Chem. Eng.* **2014**, *3*, 68.
[11] A.-L. Duchemin, H. Vignes, J. Vermot, R. Chow, *Curr. Opin. Genet. Dev.* **2019**, *57*, 106.

[12] S. Vianello, M. P. Lutolf, *Dev. Cell* **2019**, *48*, 751.
[13] L. G. Brunel, S. M. Hull, S. C. Heilshorn, *Biofabrication* **2022**, *14*, 032001.
[14] A. J. Seymour, A. D. Westerfield, V. C. Cornelius, M. A. Skylar-Scott, S. C. Heilshorn, *Biofabrication* **2022**, *14*, 022002.
[15] C. Norotte, F. S. Marga, L. E. Niklason, G. Forgacs, *Biomaterials* **2009**, *30*, 5910.
[16] A. G. Tabriz, M. A. Hermida, N. R. Leslie, W. Shu, *Biofabrication* **2015**, *7*, 045012.
[17] L. Ouyang, J. P. K. Armstrong, Y. Lin, J. P. Wojciechowski, C. Lee-Reeves, D. Hachim, K. Zhou, J. A. Burdick, M. M. Stevens, *Sci. Adv.* **2020**, *6*, eabc5529.
[18] F. Dolati, Y. Yu, Y. Zhang, A. M. De Jesus, E. A. Sander, I. T. Ozbolat, *Nanotechnology* **2014**, *25*, 145101.
[19] Q. Gao, Y. He, J. Fu, A. Liu, L. Ma, *Biomaterials* **2015**, *61*, 203.
[20] W. Jia, P. S. Gungor-Ozkerim, Y. S. Zhang, K. Yue, K. Zhu, W. Liu, Q. Pi, B. Byambaa, M. R. Dokmeci, S. R. Shin, A. Khademhosseini, *Biomaterials* **2016**, *106*, 58.
[21] W. Wu, A. DeConinck, J. A. Lewis, *Adv. Mater.* **2011**, *23*, H178.
[22] J. S. Miller, K. R. Stevens, M. T. Yang, B. M. Baker, D.-H. T. Nguyen, D. M. Cohen, E. Toro, A. A. Chen, P. A. Galie, X. Yu, R. Chaturvedi, S. N. Bhatia, C. S. Chen, *Nat. Mater.* **2012**, *11*, 768.
[23] D. B. Kolesky, R. L. Truby, A. S. Gladman, T. A. Busbee, K. A. Homan, J. A. Lewis, *Adv. Mater.* **2014**, *26*, 3124.
[24] S. Zhang, C. Qi, W. Zhang, H. Zhou, N. Wu, M. Yang, S. Meng, Z. Liu, T. Kong, *Adv. Mater.* **2023**, *35*, 2209263.
[25] L. Ouyang, J. A. Burdick, W. Sun, *ACS Appl. Mater. Interfaces* **2018**, *10*, 12424.
[26] D. F. Duarte Campos, A. Blaeser, M. Weber, J. Jäkel, S. Neuss, W. Jahnen-Dechent, H. Fischer, *Biofabrication* **2013**, *5*, 015003.
[27] D. J. Shiwarski, A. R. Hudson, J. W. Tashman, A. W. Feinberg, *APL Bioeng.* **2021**, *5*, 010904.
[28] G. Größbacher, M. Bartolf-Kopp, C. Gergely, P. N. Bernal, S. Florczak, M. de Ruijter, N. G. Rodriguez, J. Groll, J. Malda, T. Jüngst, R. Levato, *Adv. Mater.* **2023**, *35*, 2300756.
[29] C. A. Murphy, K. S. Lim, T. B. F. Woodfield, *Adv. Mater.* **2022**, *34*, 2107759.
[30] T. H. Qazi, J. A. Burdick, *Biomater. Biosyst.* **2021**, *1*, 100008.
[31] J. T. Muth, D. M. Vogt, R. L. Truby, Y. Mengüç, D. B. Kolesky, R. J. Wood, J. A. Lewis, *Adv. Mater.* **2014**, *26*, 6307.
[32] A. K. Grosskopf, R. L. Truby, H. Kim, A. Perazzo, J. A. Lewis, H. A. Stone, *ACS Appl. Mater. Interfaces* **2018**, *10*, 23353.
[33] E. Gioffredi, M. Boffito, S. Calzone, S. M. Giannitelli, A. Rainer, M. Trombetta, P. Mozetic, V. Chiono, *Procedia CIRP* **2016**, *49*, 125.
[34] D. B. Kolesky, K. A. Homan, M. A. Skylar-Scott, J. A. Lewis, *Proc. Natl. Acad. Sci. USA* **2016**, *113*, 3179.
[35] R. Suntornnond, E. Y. S. Tan, J. An, C. K. Chua, *Sci. Rep.* **2017**, *7*, 16902.
[36] H.-J. Jeong, H. Nam, J. Jang, S.-J. Lee, *Bioengineering* **2020**, *7*, 32.
[37] T. S. Mohan, P. Datta, S. Nesaei, V. Ozbolat, I. T. Ozbolat, *Prog. Biomed. Eng.* **2022**, *4*, 022003.
[38] M. W. Kassem, S. Lake, W. Roberts, S. Salandy, M. Loukas, *Transl. Res. Anat.* **2021**, *23*, 100096.
[39] F. Saremi, H. Muresian, D. Sánchez-Quintana, *RadioGraphics* **2012**, *32*, E1.
[40] J. L. Drury, D. J. Mooney, *Biomaterials* **2003**, *24*, 4337.
[41] J. M. Unagolla, A. C. Jayasuriya, *Appl. Mater. Today* **2020**, *18*, 100479.
[42] B. Guerra Silva, R. Pereira, J. Burga Sánchez, M. I. Guanipa Ortiz, F. H. Baggio-Aguiar, D. A. N. Leite Lima, *Acta Stomatol. Croat.* **2022**, *56*, 363.
[43] P. Sareło, M. Duda, M. Gąsior-Głogowska, E. Wysokińska, W. Kałas, H. Podbielska, M. Wawrzyńska, M. Kopaczyńska, *Materials* **2020**, *13*, 5634.
[44] S. C. Heilshorn, K. A. DiZio, E. R. Welsh, D. A. Tirrell, *Biomaterials* **2003**, *24*, 4245.
[45] E. Dejana, S. Colella, L. Languino, G. Balconi, C. Corbascio, P. Marchisio, *J. Cell Biol.* **1987**, *104*, 1403.
[46] J. Chen, X. Zhang, R. Millican, T. Lynd, M. Gangasani, S. Malhotra, J. Sherwood, P. T. Hwang, Y. Cho, B. C. Brott, G. Qin, H. Jo, Y.-S. Yoon, H.-W. Jun, *Front. Cardiovasc. Med.* **2021**, *8*, 790529.
[47] M. A. Bowler, W. D. Merryman, *Cardiovasc. Pathol.* **2015**, *24*, 1.
[48] A. J. Seymour, S. Shin, S. C. Heilshorn, *Adv. Healthcare Mater.* **2021**, *10*, 2100644.
[49] P. Jönsson, M. P. Jonsson, J. O. Tegenfeldt, F. Höök, *Biophys. J.* **2008**, *95*, 5334.
[50] K. Pusch, T. J. Hinton, A. W. Feinberg, *HardwareX* **2018**, *3*, 49.
[51] A. Lee, A. R. Hudson, D. J. Shiwarski, J. W. Tashman, T. J. Hinton, S. Yerneni, J. M. Bliley, P. G. Campbell, A. W. Feinberg, *Science* **2019**, *365*, 482.
[52] S. M. Hull, C. D. Lindsay, L. G. Brunel, D. J. Shiwarski, J. W. Tashman, J. G. Roth, D. Myung, A. W. Feinberg, S. C. Heilshorn, *Adv. Funct. Mater.* **2021**, *31*, 2007983.
[53] S. Shin, J. Hyun, *ACS Appl. Mater. Interfaces* **2017**, *9*, 26438.
[54] S. Shin, H. Kwak, D. Shin, J. Hyun, *Nat. Commun.* **2019**, *10*, 4650.
[55] J. Schindelin, I. Arganda-Carreras, E. Frise, V. Kaynig, M. Longair, T. Pietzsch, S. Preibisch, C. Rueden, S. Saalfeld, B. Schmid, J.-Y. Tinevez, D. J. White, V. Hartenstein, K. Eliceiri, P. Tomancak, A. Cardona, *Nat. Methods* **2012**, *9*, 676.